Journal of Computational Applied Mechanics 2025, 56(2): 488-505

DOI: 10.22059/jcamech.2024.377960.1125

RESEARCH PAPER

Elastic analysis of rotating thick cylindrical shells under linear variable pressure and bi-directional temperature loading

Fatemeh Ramezani, Mohammad Zamani Nejad *, Mehdi Jabbari

Department of Mechanical Engineering, Yasouj University, Yasouj, Iran

Abstract

In this paper, a bi-directional thermoelastic analysis of a rotating thick cylindrical shells subjected to mechanical loading is presented. The formulation is based on the first-order shear deformation theory (FSDT), which accounts for transverse shear. The governing equations, derived using the minimum total potential energy principle, are solved using the multi-layered method (MLM). Solving this set of equations, applying boundary conditions and continuity conditions between the layers, yields displacements and stresses. Finally, the displacements and stresses along the radius and length are plotted, and their distributions are compared with solutions obtained using the finite-element method (FEM). To the best of the researchers' knowledge, in the literature, there is no study carried out bi-directional thermoelastic analysis of clamped-clamped rotating thick shells under linear variable pressure in the longitudinal direction.

Keywords: Thick cylindrical, bi-directional, thermoelastic, shell, rotating, first-order shear deformation theory (FSDT), multi-layers method (MLM);

1. Introduction

Cylindrical shells are indispensable components in various industries, owing to their ability to withstand high internal pressures. Their design and analysis demand meticulous attention to ensure structural integrity and safety. Advanced analytical and computational methods play a pivotal role in optimizing these shells' performance [Fatehi and Nejad [1]; Mazarei et al. [2]; Nejad et al. [3]; Farajpour and Rastgoo [4]; Ebrahimi et al. [5]; Nejad et al. [6]; Afshin et al. [7]; Kashkoli et al. [8]; Gharibi et al. [9]; Nejad et al [10]; Kashkoli et al. [11]; Jabbari and Nejad [12]; Dindarloo and Li [13]; Taghizadeh et al. [14]; Sofiyev and Fantuzzi [15]; Taghizadeh and Nejad [16]; Jabbari and Nejad [17]]. Thermal stress analysis is crucial for designing structures and components that can withstand thermal loads [kashkoli et al. [18]; Nejad et al. [19]; Kashkoli and Nejad [20]; Nejad and Fatehi [21]; Nejad and Kashkoli [22]; Dehghan et al. [23]; Kashkoli and Nejad [24]; Nejad et al.[25]; Farajpour et al. [26]; Li et al. [27]; Nejad et al. [28]; Ghannad and Nejad [29]; Zhang and She [30]; Ramezani and Nejad [31]]. Panferov [32] presented the thermoelastic analysis on an elastic truncated conical with uniform thickness. Sundarasivarao and Ganesan [33] analysed the behavior of a conical shell under pressure using the finite element technique. Mirsky and Hermann [34] researched the analysis of thick cylindrical shells using the FSDT with uniform and isotropic materials. Witt [35] presented a thermal stress analysis for a conical shell under axis-symmetric temperature distributions. Jane and Wu [36] employed a generalized thermoelasticity problem using the curvilinear circular conical coordinate system. Eipakchi et al. [37] employed a mathematical approach to analyze the elasticity of a thick conical shell with varying thickness

* Corresponding author. *E-mail address:* m.zamani.n@gmail.com

using perturbation theory under non-uniform internal pressure. Nejad and Rahimi [38] investigated deformations and stresses in FGM pressurized thick hollow cylinder based on closed form solutions for one-dimensional steady-state thermal stresses. Ghannad et al. [39] studied the elastic analysis of thick truncated conical shells with uniform thickness. Jabbari et al. [40] presented a thermo-elastic analysis of a rotating truncated conical shell subjected to temperature, internal pressure, and external pressure by using the FSDT and MLM. They derived a solution for the problem by reducing it to a reverse thermo-elasticity problem. Ghannad and Nejad [41] studied elastic solution of pressurized clamped-clamped thick cylindrical shells made of FGMs based on the FSDT. Eipakchi [42] studied the determination of displacements and stresses in a homogeneous thick conical shell based on the third-order shear deformation theory under non-uniform internal pressure, using perturbation theory. Ghannad et al. [43] presented displacement and stress analyses for pressurized thick cylindrical shells using perturbation techniques. Nejad et al. [44] analyzed a mathematical solution that partially uses analysis and partially uses numerical methods to calculate the displacements and stresses in a cylindrical shell with varying thickness under a non-uniform pressure They systematically examined how the primary factors of the problem affect displacement and stress levels. Civalek [45] studied the free vibration analysis of isotropic laminated conical shells using the numerical solution of the governing differential equations of motion based on shear deformation theory. Nejad et al. [46] presented an analytical and numerical solution for truncated conical shells based on the First Shear Deformation Theory. Nejad et al. [47] studied a semi-analytical solution for a cylindrical shell with variable thickness based on the First Shear Deformation Theory under uniform pressure. Ghannad et al. [48] obtained a semi-analytical solution to determine displacements and stresses in a thick cylindrical shell using the First Shear Deformation Theory based on disk form multilayers under uniform pressure. Jabbari et al. [49] conducted a thermo-elastic analysis on a vessel made of Functionally Graded Material (FGM) subjected to temperature gradient and internal non-uniform pressure using a higher-order shear deformation theory. Nejad et al. [50] presented semi-analytically a rotating thick hollow cylinder made of Functionally Graded Material under arbitrarily non-uniform pressure using the FSDT. Jabbari et al. [51] conducted a thermoelastic analysis on a thick truncated conical shell under a temperature gradient and non-uniform internal pressure using disk-form multilayers based on the first shear deformation theory. Kashkoli [52] obtained a thermomechanical solution for creep analysis of FG thick cylindrical shells with variable thickness using the FSDT and MLM. Hamzah et al. [53] analyzed the vibration characteristics of cylindrical shells under varying ambient temperatures using Finite Element Method (FEM). Ghannad et al. [54] studied the analytical solution of pressurized thick cylindrical shells with variable thickness based on the FSDT and using the asymptotic method (MAM) of the perturbation theory. Aghaienezhad et al. [55] studied the behavior of spherical and cylindrical shells subjected to external pressure using the Generalized Differential Quadrature (GDQ) method. Nejad et al. [56] studied thermo-elastic analysis in a FG thick shell of revolution with arbitrary curvature and variable thickness based on higher-order shear deformation theory. Ifayefunmi and Ruan [57] presented the buckling analysis of stiffened Cone–Cylinder Structures under axial compressive load using a computational finite element (FE) code. Gharooni et al. [58] investigated an analytical solution in axisymmetric clamped-clamped thick cylindrical shells made of FGM Using the third-order shear deformation theory. Ramezani et al. [59] presented a thermoelastic analysis of cylindrical pressure vessels under bi-directional temperature gradients based on FSDT. Nejad et al. [60] studied the semi-analytical solution for FG thick truncated conical shells under non-uniform pressure loading, utilizing the FSDT and the MLM. Ramezani et al. [61] presented the thermoelastic analysis of pressurized thick cylindrical shell with nonlinear variable thickness based on FSDT. Mannani et al. [62] investigated mechanical stress and deformation analyses on a cylindrical shell under mechanical loads using a higher-order sinusoidal shear deformation theory and thickness stretching formulation.

The current study investigates thermoelastic analysis for rotating clamped-clamped thick-walled cylinders under internal linear variable pressure and bi-directional thermal loading. For the semi-analytical investigation, FSDT and disk-form multilayer methods are utilized. The analytical results are compared with those obtained from the finite element method, demonstrating good agreement.

2. Problem formulation

First, the thermoelastic analysis of thick cylindrical shells with clamped-clamped conditions at the both ends, subjected to internal pressure $P_{in}(x)$, and rotating around its axis with a constant angular velocity (ω), is shown in Fig 1.

where thickness (h) and length (L), and (R) represent the distance of middle surface from the axial direction. Also, z is the distance of typical point from the middle surface.

$$r = R + z \tag{1}$$

$$R = R_i + \frac{h}{2} \tag{2}$$

where R_i represent inner radius. with respect to Fig 1, x and z must be as follows:

$$\begin{cases} 0 \le x \le L \\ -\dfrac{h}{2} \le z \le \dfrac{h}{2} \end{cases} \tag{3}$$

The general axisymmetric displacement field, (U_x, U_z), in the FSDT could be expressed on the basis of axial and radial displacements as follows:

$$\begin{Bmatrix} U_x \\ U_z \end{Bmatrix} = \begin{Bmatrix} u_0(x) \\ w_0(x) \end{Bmatrix} + \begin{Bmatrix} u_1(x) \\ w_1(x) \end{Bmatrix} z \tag{4}$$

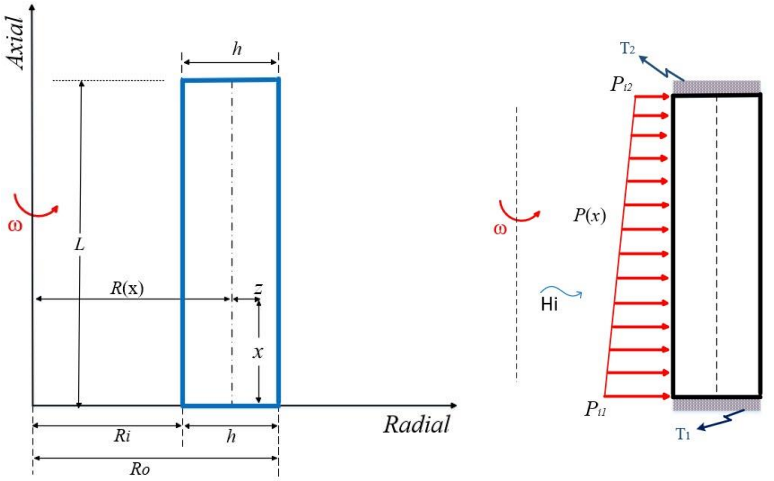

Fig 1: cross section of the rotating thick cylindrical shells with clamped–clamped ends

where $u_0(x)$ and $w_0(x)$ are the displacement components of the middle surface. Also, $u_1(x)$ and $w_1(x)$ are the functions used to determine the displacement field.

Due to the influence of $(\partial/\partial\theta)=0$, the temperature distribution function within the cylindrical shell can be expressed solely as a function of the radial coordinate (r) and the axial coordinate (x), therefore

$$T = T(x, z) \tag{5}$$

The temperature field for this cylindrical shell using the first-order temperature theory (FTT) is may expressed according to $\Theta(z, x)$ as:

$$\Theta(x, z) = T - T^* = \Theta^0(x) + z\Theta^1(x) = \Theta^0 + z\Theta^1 \tag{6}$$

where T^* is the reference temperature. Also, Θ^0 and Θ^1 denote the temperature variations relative to a reference temperature. The strain–displacement relations in the cylindrical coordinates system are

$$\begin{cases} \varepsilon_x = \dfrac{\partial U_x}{\partial x} = \dfrac{du_0}{dx} + \dfrac{du_1}{dx} z \\ \varepsilon_\theta = \dfrac{U_z}{r} = \dfrac{1}{R+z}(w_0 + w_1 z) \\ \varepsilon_z = \dfrac{\partial U_z}{\partial z} = w_1 \\ \gamma_{xz} = \dfrac{\partial U_x}{\partial z} + \dfrac{\partial U_z}{\partial x} = \left(u_1 + \dfrac{dw_0}{dx}\right) + \dfrac{dw_1}{dx} z \end{cases} \tag{7}$$

The thermal field-temperature change relations are

$$\begin{cases} e_z = -\dfrac{\partial \Theta(x,z)}{\partial z} = -\Theta^1(x) \\ e_\theta = 0 \\ e_x = -\dfrac{\partial \Theta(x,z)}{\partial x} = -\dfrac{d\Theta^0(x)}{dx} - \dfrac{d\Theta^1(x)}{dx} z \end{cases} \tag{8}$$

In addition, the stress tensor and heat flux vector components can be written as

$$\begin{aligned} &\sigma_i = \lambda E\left[(1-\nu)\varepsilon_i + \nu\left(\varepsilon_j + \varepsilon_k\right)\right] - \lambda\alpha(1+\nu)T, \qquad \mathrm{i} \neq \mathrm{j} \neq \mathrm{k} \\ &\tau_{xz} = \lambda E\left[(1-2\nu)\frac{\gamma_{xz}}{2}\right] \end{aligned} \tag{9}$$

where

$$\lambda = \frac{1}{(1+\nu)(1-2\nu)} \tag{10}$$

$$\begin{bmatrix} q_z \\ q_x \end{bmatrix} = \begin{bmatrix} K & 0 \\ 0 & K \end{bmatrix} \begin{bmatrix} e_z \\ e_x \end{bmatrix} \tag{11}$$

Here, σ_i, ε_i, q_i and e_i are the components of stress tensor, strain tensor, heat flux vector and, thermal field vector in the axial (x), circumferential (θ) and radial (z) directions (τ_{xz} is the shear stress). Also, K is the thermal conduction coefficient. The stress resultants in terms of mechanical (index m) and thermal (index t) stress resultants are:

$$\begin{Bmatrix} N_z^m \\ N_\theta^m \\ N_x^m \end{Bmatrix} = \int_{-h/2}^{h/2} \begin{Bmatrix} \sigma_z(1+\dfrac{z}{R}) \\ \sigma_\theta \\ \sigma_x(1+\dfrac{z}{R}) \end{Bmatrix} dz$$

$$\begin{Bmatrix} M_\theta^m \\ M_x^m \end{Bmatrix} = \int_{-h/2}^{h/2} \begin{Bmatrix} \sigma_\theta \\ \sigma_x(1+\dfrac{z}{R}) \end{Bmatrix} z dz$$

$$\begin{Bmatrix} Q_x^m \\ M_{zx}^m \end{Bmatrix} = \mathrm{k} \int_{-h/2}^{h/2} \begin{Bmatrix} 1 \\ z \end{Bmatrix} \tau_{zx}\left(1+\frac{z}{R}\right) dz$$

$$\begin{Bmatrix} N_z^t \\ N_x^t \end{Bmatrix} = \int_{-h/2}^{h/2} \begin{Bmatrix} q_z \\ q_x \end{Bmatrix} \left(1+\frac{z}{R}\right) dz$$

$$M_z^t = \int_{-h/2}^{h/2} h_x \left(1+\frac{z}{R}\right) z dz \tag{12}$$

where k represents a correction factor incorporated into the shear stress term. In the static state, this correction is applied for cylindrical shells $\mathrm{k} = 5/6$ [63].

According to the principle of virtual work, the changes in strain energy are equivalent to the changes in external work done, as expressed below:

$$\delta U = \delta W \tag{13}$$

where U is the total strain energy of the elastic body and W is the total work of external forces due to internal pressure and centrifugal force. By substituting strain energy and the work of external forces:

$$\delta U = \int_0^L \int_0^{2\pi} \int_{-h/2}^{h/2} \frac{1}{2} \begin{pmatrix} \sigma_z \delta\varepsilon_z + \sigma_\theta \delta\varepsilon_\theta + \sigma_x \delta\varepsilon_x \\ + \tau_{zx} \delta\gamma_{zx} - q_x \delta e_x - q_z \delta e_z \end{pmatrix} (R+z) dz d\theta dx \tag{14}$$

$$\partial W = \int_0^L \int_0^{2\pi} \left(\left(P\delta U_Z - H_i \delta\Theta \right) \left(R - \frac{h}{2} \right) + H_O \delta\Theta \left(R + \frac{h}{2} \right) \right) dx d\theta \tag{15}$$

By substituting Eqs. (14)-(15) into Eq. (13) the governing equations are obtained as:

$$\begin{cases} -\frac{d}{dx}\left(RN_x^m \right) = 0 \\ RQ_x^m - \frac{d}{dx}\left(RM_x^m \right) = 0 \\ RN_z^m - \frac{d}{dx}\left(RM_{zx}^m \right) + M_\theta^m = -P\frac{h}{2}\left(R - \frac{h}{2} \right) + \frac{\rho\omega^2}{6} Rh^3 \\ N_\theta^m - \frac{d}{dx}\left(RQ_x^m \right) = P\left(R - \frac{h}{2} \right) + \frac{\rho\omega^2}{6}\frac{h}{2}\left(12R^2 + h^2 \right) \\ -\frac{d}{dx}\left(RN_x^t \right) = H_0\left(R + \frac{h}{2} \right) - H_i\left(R - \frac{h}{2} \right) \\ RN_z^t - \frac{d}{dx}\left(RM_x^t \right) = H_i\frac{h}{2}\left(R - \frac{h}{2} \right) + H_o\left(R + \frac{h}{2} \right) \end{cases} \tag{16}$$

Also, the boundary conditions are:

$$\left[N_x^m \delta u + M_x^m \delta\varphi + Q_x^m \delta w + M_{zx}^m \delta\psi + N_x^t \delta\Theta^0(x) + M_x^t \delta\Theta^1(x) \right]\Big|_{0,L} = 0 \tag{17}$$

Due to the irreversibility of $[A_3]$ and the necessity of its inverse for further calculations, it is essential to perform two variable changes in the solution process.

$$u = \int \frac{du_0}{dx} dx + C_0 \tag{18}$$

$$\Theta^0 = \int \frac{d\Theta^0}{dx} dx + C_1 \tag{19}$$

Implementing two variable changes necessitates integrating the equations associated with these variables within the system of differential equations. By substituting Eq. (12) into Eq. (16), the system of differential equations in Eq. (16) can be reformulated as follows:

$$[A_1]\frac{d^2}{dx^2}\{\bar{y}\} + [A_2]\frac{d}{dx}\{\bar{y}\} + [A_3]\{\bar{y}\} = [F] \tag{20}$$

$$\{\bar{y}\} = \left\{ \frac{du_0}{dx}, u, w_0, w_1, \frac{d\Theta^0}{dx}, \Theta^1 \right\} \tag{21}$$

where $[A_1]_{6\times6}, [A_2]_{6\times6}, [A_3]_{6\times6}$ are the coefficients matrices, and F is the force vector, as:

$$[A_1] = \begin{bmatrix} 0 & 0 & 0 \\ 0 & -\frac{E(1-\nu)}{(1-2\nu)(1+\nu)} R\frac{h^3}{12} & 0 \\ 0 & 0 & -\mathrm{k}\frac{E}{2(1+\nu)} Rh \\ 0 & 0 & -\mathrm{k}\frac{E}{2(1+\nu)}\frac{h^3}{12} \\ 0 & 0 & 0 \\ 0 & 0 & 0 \end{bmatrix}$$

$$\begin{bmatrix} 0 & 0 & 0 \\ 0 & 0 & 0 \\ -\mathrm{k}\dfrac{E}{2(1+\nu)}\dfrac{h^3}{12} & 0 & 0 \\ -\mathrm{k}\dfrac{E}{2(1+\nu)}R\dfrac{h^3}{12} & 0 & 0 \\ 0 & 0 & 0 \\ 0 & R\int\limits_{-h/2}^{h/2} Kzdz & \int\limits_{-h/2}^{h/2} Kz^3dz \end{bmatrix} \tag{22}$$

$$[A_2]=\begin{bmatrix} 0 & \dfrac{E(1-\nu)}{(1-2\nu)(1+\nu)}\dfrac{h^3}{12} & 0 \\ -\dfrac{E(1-\nu)}{(1-2\nu)(1+\nu)}\dfrac{h^3}{12} & -\dfrac{(1-\nu)}{(1-2\nu)(1+\nu)}\dfrac{h^2}{12}\left(3R\dfrac{dh}{dx}+h\dfrac{dR}{dx}\right) & \mathrm{k}\dfrac{E}{2(1+\nu)}Rh \\ 0 & -\mathrm{k}\dfrac{E}{2(1+\nu)}Rh & -\dfrac{\mathrm{k}}{2(1+\nu)}\left(RE\dfrac{dh}{dx}+hE\dfrac{dR}{dx}\right) \\ 0 & \dfrac{E}{(1+\nu)}\dfrac{h^3}{12}\left(\dfrac{2\nu}{(1-2\nu)}-\dfrac{\mathrm{k}}{2}\right) & -\dfrac{\mathrm{k}E}{2(1+\nu)}\dfrac{h^2}{4}\dfrac{dh}{dx} \\ 0 & 0 & 0 \\ 0 & 0 & 0 \end{bmatrix}$$

$$\begin{bmatrix} 0 & 0 & 0 \\ \dfrac{E}{(1+\nu)}\dfrac{h^3}{12}\left(\dfrac{\mathrm{k}}{2}-\dfrac{\nu}{(1-2\nu)}\right) & \dfrac{E(1+\nu)}{(1-2\nu)(1+\nu)}\dfrac{h^3}{12}\alpha & \dfrac{E(1+\nu)}{(1-2\nu)(1+\nu)}R\dfrac{h^3}{12}\alpha \\ -\dfrac{\mathrm{k}E}{2(1+\nu)}\dfrac{h^2}{4}\dfrac{dh}{dx} & 0 & 0 \\ -\dfrac{\mathrm{k}}{2(1+\nu)}\dfrac{h^2}{12}\left(hE\dfrac{dR}{dx}+3RE\dfrac{dh}{dx}\right) & 0 & 0 \\ 0 & 0 & 0 \\ 0 & \dfrac{dR}{dx}\int\limits_{-h/2}^{h/2} Kzdz & 0 \end{bmatrix} \tag{23}$$

$$[A_3]=\begin{bmatrix} \dfrac{E(1-\nu)}{(1-2\nu)(1+\nu)}Rh & 0 & \dfrac{E\nu}{(1-2\nu)(1+\nu)}h \\ -\dfrac{E(1-\nu)}{(1-2\nu)(1+\nu)}\dfrac{h^2}{4}\dfrac{dh}{dx} & \mathrm{k}\dfrac{E}{2(1+\nu)}Rh & 0 \\ \dfrac{E\nu}{(1-2\nu)(1+\nu)}h & -\dfrac{\mathrm{k}E}{2(1+\nu)}\left(R\dfrac{dh}{dx}+h\dfrac{dR}{dx}\right) & \dfrac{E(1-\nu)}{(1-2\nu)(1+\nu)}\ln\left(\dfrac{R+\dfrac{h}{2}}{R-\dfrac{h}{2}}\right) \\ \dfrac{E\nu}{(1-2\nu)(1+\nu)}Rh & -\dfrac{\mathrm{k}E}{2(1+\nu)}\dfrac{h^2}{4}\dfrac{dh}{dx} & \dfrac{E}{(1-2\nu)(1+\nu)}\left(h-(1-\nu)R\ln\left(\dfrac{R+\dfrac{h}{2}}{R-\dfrac{h}{2}}\right)\right) \\ 0 & 0 & 0 \\ 0 & 0 & 0 \end{bmatrix}$$

$$\begin{bmatrix}
\frac{E\nu}{(1-2\nu)(1+\nu)}Rh & -\frac{E(1+\nu)}{(1-2\nu)(1+\nu)}Rh\alpha & -\frac{E(1+\nu)}{(1-2\nu)(1+\nu)}\frac{h^3}{12}\alpha \\
\frac{E\nu}{(1-2\nu)(1+\nu)}\frac{h^2}{2}\frac{dh}{dx} & \frac{(1+\nu)}{(1-2\nu)(1+\nu)}\frac{h^2}{12}\left(3\alpha E\frac{dh}{dx}+hE\frac{d\alpha}{dx}\right) & \frac{(1+\nu)}{(1-2\nu)(1+\nu)}\frac{h^2}{12}\left(3\alpha ER\frac{dh}{dx}+hER\frac{d\alpha}{dx}+\alpha Eh\frac{dR}{dx}\right) \\
-\frac{E}{(1-2\nu)(1+\nu)}\left(h-(1-\nu)R\ln\left(\frac{R+\frac{h}{2}}{R-\frac{h}{2}}\right)\right) & -\frac{E(1+\nu)}{(1-2\nu)(1+\nu)}h\alpha & 0 \\
\frac{E(1-\nu)}{(1-2\nu)(1+\nu)}R^3\ln\left(\frac{R+\frac{h}{2}}{R-\frac{h}{2}}\right) & -\frac{E(1+\nu)}{(1-2\nu)(1+\nu)}Rh\alpha & -\frac{E(1+\nu)}{(1-2\nu)(1+\nu)}\frac{h^3}{6}\alpha \\
0 & -R\int_{-h/2}^{h/2}K dz & -\int_{-h/2}^{h/2}Kz^2 dz \\
0 & 0 & -\int_{-h/2}^{h/2}K(R+z)dz
\end{bmatrix} \tag{24}$$

$$[F]=\begin{Bmatrix}
C_1 \\
0 \\
P\frac{h}{2}\left(R-\frac{h}{2}\right)+\frac{\rho\omega^2}{6}Rh^3 \\
-P\left(R-\frac{h}{2}\right)+\frac{\rho\omega^2}{6}\frac{h}{2}\left(12R^2+h^2\right) \\
\left[H_o\left(R-\frac{h}{2}\right)-H_i\left(R+\frac{h}{2}\right)\right]x+C_2 \\
\frac{h}{2}\left[H_i\left(R-\frac{h}{2}\right)+H_o\left(R+\frac{h}{2}\right)\right]
\end{Bmatrix} \tag{25}$$

3. Semi-analytical solution

Eqs. (16) and (17) consist of a set of non-homogeneous linear differential equations with variable coefficients. Obtaining an analytical solution for this set appears to be highly challenging, if not outright impossible. Therefore, this study introduces a semi-analytical method called the Multilayer Method to solve Eq. (16). In this approach, a cylinder under two-dimensional thermal analysis is segmented into homogeneous disk layers, each with a constant thickness $h^{[k]}$ (see Fig 2). Consequently, the governing equations are converted into a non-homogeneous set of differential equations with constant coefficients. Here, $x^{[k]}$ and $R^{[k]}$ represent the length and radius at the midpoint of the disks, respectively. The variable k denotes the specific disk number, and n_d represents the total number of disks.

The length of middle $x^{[k]}$ of kth disk (see Fig 2) is as follows

$$\left(x^{[k]}-\frac{t}{2}\right)\le x\le\left(x^{[k]}+\frac{t}{2}\right),\qquad x^{[k]}=t\left(k-\frac{1}{2}\right)\quad\&\quad t=\frac{L}{n} \tag{26}$$

Based on the mentioned assumptions, the governing equations for each homogeneous disk are obtained as follows:

$$\left[A_1\right]^{[k]}\frac{d^2}{dx^2}\{\bar{y}\}^{[k]}+\left[A_2\right]^{[k]}\frac{d}{dx}\{\bar{y}\}^{[k]}+\left[A_3\right]^{[k]}\{\bar{y}\}^{[k]}=[F]^{[k]} \tag{27}$$

$$\{\bar{y}\}^{[k]}=\left\{\left(\frac{du_0}{dx}\right)^{[k]},u_1^{[k]},w_0^{[k]},w_1^{[k]},\left(\frac{d\Theta^0}{dx}\right)^{[k]},\Theta^{1[k]}\right\}^T \tag{28}$$

where, the coefficients matrices, $\left[A_i\right]_{6\times6}^{[k]}$ and force vector, $\{F\}_{6\times6}^{[k]}$ are as follows:

$$\left[A_1\right]^{[k]}=\begin{bmatrix} 0 & 0 & 0 \\ 0 & -\dfrac{E(1-\nu)}{(1-2\nu)(1+\nu)}R^{[k]}\dfrac{h^{[k]3}}{12} & 0 \\ 0 & 0 & -\mathrm{k}\dfrac{E}{2(1+\nu)}R^{[k]}{}_h{}^{[k]} \\ 0 & 0 & -\mathrm{k}\dfrac{E}{2(1+\nu)}\dfrac{h^{[k]3}}{12} \\ 0 & 0 & 0 \\ 0 & 0 & 0 \end{bmatrix}$$

$$\begin{bmatrix} 0 & 0 & 0 \\ 0 & 0 & 0 \\ -\mathrm{k}\dfrac{E}{2(1+\nu)}\dfrac{h^{[k]3}}{12} & 0 & 0 \\ -\mathrm{k}\dfrac{E}{2(1+\nu)}R^{[k]}\dfrac{h^{[k]3}}{12} & 0 & 0 \\ 0 & 0 & 0 \\ 0 & R^{[k]}\int\limits_{-h^{[k]}/2}^{h^{[k]}/2}Kzdz & \int\limits_{-h^{[k]}/2}^{h^{[k]}/2}Kz^3dz \end{bmatrix} \tag{29}$$

$$\left[A_2\right]^{[k]}=\begin{bmatrix} 0 & \dfrac{E(1-\nu)}{(1-2\nu)(1+\nu)}\dfrac{h^{[k]3}}{12} & 0 \\ -\dfrac{E(1-\nu)}{(1-2\nu)(1+\nu)}\dfrac{h^{[k]3}}{12} & -\dfrac{(1-\nu)}{(1-2\nu)(1+\nu)}\dfrac{h^{[k]2}}{12}\left(3R^{[k]}\dfrac{dh^{[k]}}{dx}+h^{[k]}\dfrac{dR^{[k]}}{dx}\right) & \mathrm{k}\dfrac{E}{2(1+\nu)}R^{[k]}{}_h{}^{[k]} \\ 0 & -\mathrm{k}\dfrac{E}{2(1+\nu)}R^{[k]}{}_h{}^{[k]} & -\dfrac{\mathrm{k}}{2(1+\nu)}\left(R^{[k]}E\dfrac{dh^{[k]}}{dx}+hE\dfrac{dR^{[k]}}{dx}\right) \\ 0 & \dfrac{E}{(1+\nu)}\dfrac{h^{[k]3}}{12}\left(\dfrac{2\nu}{(1-2\nu)}-\dfrac{\mathrm{k}}{2}\right) & -\dfrac{\mathrm{k}E}{2(1+\nu)}\dfrac{h^{[k]2}}{4}\dfrac{dh^{[k]}}{dx} \\ 0 & 0 & 0 \\ 0 & 0 & 0 \end{bmatrix}$$

$$\begin{bmatrix} 0 & 0 & 0 \\ \frac{E}{(1+\nu)}\frac{h^{[k]3}}{12}\left(\frac{\mathrm{k}}{2}-\frac{\nu}{(1-2\nu)}\right) & \frac{E(1+\nu)}{(1-2\nu)(1+\nu)}\frac{h^{[k]3}}{12}\alpha & \frac{E(1+\nu)}{(1-2\nu)(1+\nu)}R\frac{h^{[k]3}}{12}\alpha \\ -\frac{\mathrm{k}E}{2(1+\nu)}\frac{h^{[k]2}}{4}\frac{dh^{[k]}}{dx} & 0 & 0 \\ -\frac{\mathrm{k}}{2(1+\nu)}\frac{h^{[k]2}}{12}\left(h^{[k]}E\frac{dR^{[k]}}{dx}+3R^{[k]}E\frac{dh^{[k]}}{dx}\right) & 0 & 0 \\ 0 & 0 & 0 \\ 0 & \frac{dR^{[k]}}{dx}\int_{-h^{[k]}/2}^{h^{[k]}/2}Kzdz & 0 \end{bmatrix} \tag{30}$$

$$\left[A_3\right]^{[k]} = \begin{bmatrix} \frac{E(1-\nu)}{(1-2\nu)(1+\nu)}R^{[k]}{}_h{}^{[k]} & 0 & \frac{E\nu}{(1-2\nu)(1+\nu)}h^{[k]} \\ -\frac{E(1-\nu)}{(1-2\nu)(1+\nu)}\frac{h^{[k]2}}{4}\frac{dh^{[k]}}{dx} & \mathrm{k}\frac{E}{2(1+\nu)}R^{[k]}{}_h{}^{[k]} & 0 \\ \frac{E\nu}{(1-2\nu)(1+\nu)}h^{[k]} & -\frac{\mathrm{k}E}{2(1+\nu)}\left(R\frac{dh^{[k]}}{dx}+h\frac{dR^{[k]}}{dx}\right) & \frac{E(1-\nu)}{(1-2\nu)(1+\nu)}\ln\left(\frac{R+\frac{h^{[k]}}{2}}{R-\frac{h^{[k]}}{2}}\right) \\ \frac{E\nu}{(1-2\nu)(1+\nu)}R^{[k]}{}_h{}^{[k]} & -\frac{\mathrm{k}E}{2(1+\nu)}\frac{h^{[k]2}}{4}\frac{dh^{[k]}}{dx} & \frac{E}{(1-2\nu)(1+\nu)}\left(h^{[k]}-(1-\nu)R^{[k]}\ln\left(\frac{R^{[k]}+\frac{h^{[k]}}{2}}{R^{[k]}-\frac{h^{[k]}}{2}}\right)\right) \\ 0 & 0 & 0 \\ 0 & 0 & 0 \end{bmatrix}$$

$$\begin{bmatrix} \frac{E\nu}{(1-2\nu)(1+\nu)}R^{[k]}{}_h{}^{[k]} & -\frac{E(1+\nu)}{(1-2\nu)(1+\nu)}R^{[k]}{}_h{}^{[k]}\alpha^{[k]} & -\frac{E(1+\nu)}{(1-2\nu)(1+\nu)}\frac{h^{[k]3}}{12}\alpha^{[k]} \\ \frac{E\nu}{(1-2\nu)(1+\nu)}\frac{h^{[k]2}}{2}\frac{dh^{[k]}}{dx} & \frac{(1+\nu)}{(1-2\nu)(1+\nu)}\frac{h^{[k]2}}{12}\left(3\alpha^{[k]}E\frac{dh^{[k]}}{dx}+h^{[k]}E\frac{d\alpha^{[k]}}{dx}\right) & \frac{(1+\nu)}{(1-2\nu)(1+\nu)}\frac{h^{[k]2}}{12}\left(3\alpha^{[k]}ER^{[k]}\frac{dh^{[k]}}{dx}+h^{[k]}ER^{[k]}\frac{d\alpha^{[k]}}{dx}+\alpha^{[k]}Eh^{[k]}\frac{dR^{[k]}}{dx}\right) \\ -\frac{E}{(1-2\nu)(1+\nu)}\left(h^{[k]}-(1-\nu)R^{[k]}\ln\left(\frac{R^{[k]}+\frac{h^{[k]}}{2}}{R-\frac{h^{[k]}}{2}}\right)\right) & -\frac{E(1+\nu)}{(1-2\nu)(1+\nu)}h^{[k]}\alpha^{[k]} & 0 \\ \frac{E(1-\nu)}{(1-2\nu)(1+\nu)}R^{[k]3}\ln\left(\frac{R^{[k]}+\frac{h^{[k]}}{2}}{R^{[k]}-\frac{h^{[k]}}{2}}\right) & -\frac{E(1+\nu)}{(1-2\nu)(1+\nu)}R^{[k]}{}_h{}^{[k]}\alpha^{[k]} & -\frac{E(1+\nu)}{(1-2\nu)(1+\nu)}\frac{h^{[k]3}}{6}\alpha^{[k]} \\ 0 & -R^{[k]}\int_{-h^{[k]}/2}^{h^{[k]}/2}Kdz & -\int_{-h^{[k]}/2}^{h^{[k]}/2}Kz^2dz \\ 0 & 0 & -\int_{-h^{[k]}/2}^{h^{[k]}/2}K(R+z)dz \end{bmatrix} \tag{31}$$

$$[F]^{[k]} = \begin{Bmatrix} C_1 \\ 0 \\ P\frac{h^{[k]}}{2}\left(R^{[k]} - \frac{h^{[k]}}{2}\right) + \frac{\rho\omega^2}{6}R^{[k]}{}_h[k]^3 \\ -P\left(R^{[k]} - \frac{h^{[k]}}{2}\right) + \frac{\rho\omega^2}{6}\frac{h^{[k]}}{2}\left(12R^{[k]2} + h^{[k]2}\right) \\ \left[H_o\left(R^{[k]} - \frac{h^{[k]}}{2}\right) - H_i\left(R^{[k]} + \frac{h^{[k]}}{2}\right)\right]x + C_2 \\ \frac{h^{[k]}}{2}\left[H_i\left(R^{[k]} - \frac{h^{[k]}}{2}\right) + H_o\left(R^{[k]} + \frac{h^{[k]}}{2}\right)\right] \end{Bmatrix} \quad (32)$$

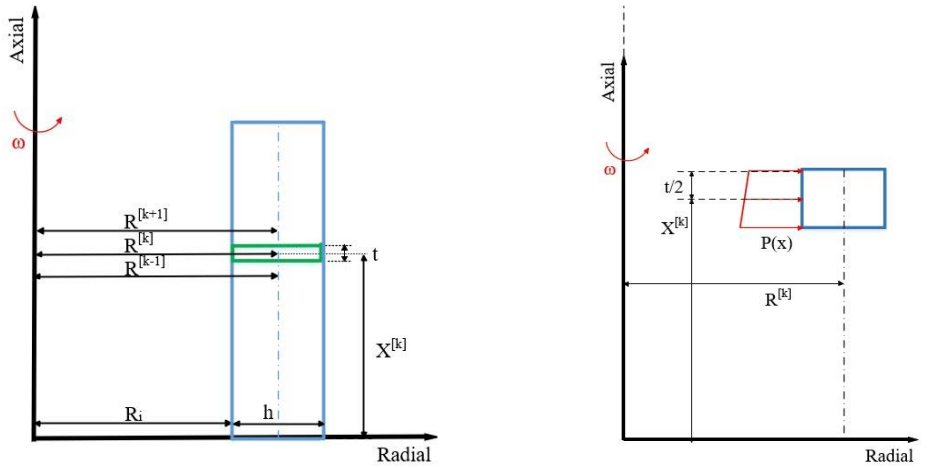

Fig 2: division of cylindrical shell into homogenous disks with constant thickness

4. Boundary and continuity conditions

In this problem, the boundary conditions of the cylinder are clamped–clamped ends subjected to temperature are:

$$\begin{Bmatrix} u_0, u_1 \\ w_0, w_1 \\ \Theta^0 \\ \Theta^1 \end{Bmatrix}_{x=0} = \begin{Bmatrix} u_0, u_1 \\ w_0, w_1 \\ \Theta^0 \\ \Theta^1 \end{Bmatrix}_{x=L} = \begin{Bmatrix} 0 \\ 0 \\ T - T_{ref} \\ 0 \end{Bmatrix} \quad (33)$$

At the boundary between the two layers in the cylinder, due to the overall homogeneity and continuity, forces, stresses, and displacements must be continuous. Given that the shear deformation theory applied is an approximation of one order and all equations related to stresses include the first derivatives of displacement, the specific continuity conditions are as follows:

$$\begin{Bmatrix} U_x^{[k-1]}(x,z) \\ U_z^{[k-1]}(x,z) \end{Bmatrix}_{x=x^{[k-1]}+\frac{t}{2}} = \begin{Bmatrix} U_x^{[k]}(x,z) \\ U_z^{[k]}(x,z) \end{Bmatrix}_{x=x^{[k]}-\frac{t}{2}} \quad (34)$$

$$\left\{\begin{matrix} U_x^{[k]}(x,z) \\ U_z^{[k]}(x,z) \end{matrix}\right\}_{x=x^{[k]}+\frac{t}{2}} = \left\{\begin{matrix} U_x^{[k+1]}(x,z) \\ U_z^{[k+1]}(x,z) \end{matrix}\right\}_{x=x^{[k+1]}-\frac{t}{2}} \tag{35}$$

and

$$\left\{\begin{matrix} \frac{dU_x^{[k-1]}(x,z)}{dx} \\ \frac{dU_z^{[k-1]}(x,z)}{dx} \end{matrix}\right\}_{x=x^{[k-1]}+\frac{t}{2}} = \left\{\begin{matrix} \frac{dU_x^{[k]}(x,z)}{dx} \\ \frac{dU_z^{[k]}(x,z)}{dx} \end{matrix}\right\}_{x=x^{[k]}-\frac{t}{2}} \tag{36}$$

$$\left\{\begin{matrix} \frac{dU_x^{[k]}(x,z)}{dx} \\ \frac{dU_z^{[k]}(x,z)}{dx} \end{matrix}\right\}_{x=x^{[k]}+\frac{t}{2}} = \left\{\begin{matrix} \frac{dU_x^{[k+1]}(x,z)}{dx} \\ \frac{dU_z^{[k+1]}(x,z)}{dx} \end{matrix}\right\}_{x=x^{[k+1]}-\frac{t}{2}} \tag{37}$$

According to the continuity conditions, 12 equations are derived. Generally, if the shell is segmented into *n* disk layers,1 $12(n-1)$ equations are obtained. By incorporating the boundary condition equations, the total becomes $12n$ equations. Solving these equations provides $12n$ unknown constants.

5. Results and discussion

In a case study, a clamped-clamped cylindrical shell with parameters $R_i = 100$ mm, $R_o = 120$ mm, h = 20 mm, and $L = 1000$ mm is analyzed. For both analytical and numerical results, the material properties $E = 395$ GPa, $\alpha = 4.3\times10^{-6}$ °C, $\rho = 19300$ Kg/m^3, $K = 175$ W/m °c and $\nu = 0.3$ are considered. $H_i = 150$ W/m^2 and along x with an internal pressure applied at $x = 0$ and $x = L$ is $P_{i1} = 160$ MPa and $P_{i2} = 60$ MPa , respectively. To achieve result convergence using the MLM, up to 70 layers were evaluated. It was found that increasing the number of layers beyond this point did not enhance the accuracy of the results. The MLM results were compared with those from the FEM in terms of displacement and stress. Fig 3 illustrates the radial displacement along the longitudinal direction within the intermediate layer, showing a comparison with FEM results. The radial displacement values indicate good agreement between the semi-analytical and numerical methods. Displacement is normalized by dividing to the internal radii. In order to normalize stresses, the mean internal pressure parameter is defined as follows:

$$\bar{P} = \frac{P_{i1} + P_{i2}}{2} \tag{38}$$

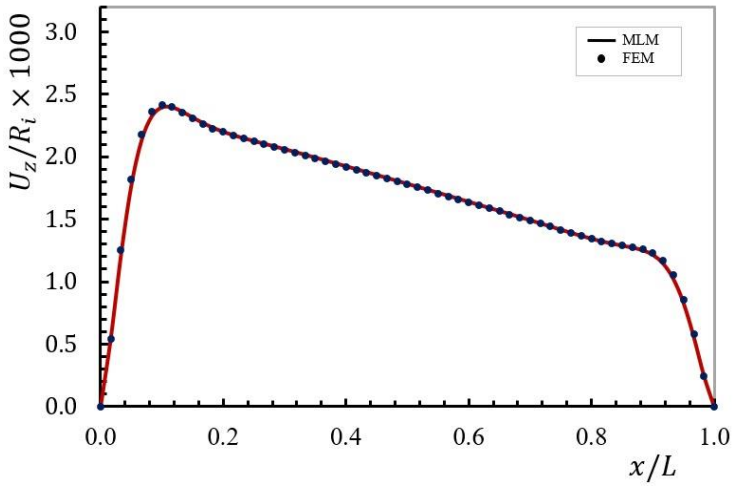

Fig 3: normalized radial displacement distribution ($\omega = 500$ rad/s)

Fig 4 presents the circumferential stress distribution along the length of the intermediate layer, measured at points distant from the boundary. The comparison between the results obtained from the FEM and another method demonstrates a good correlation.

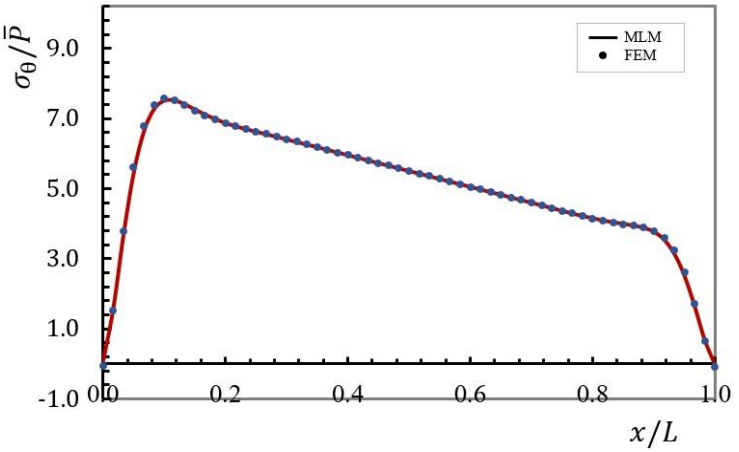

Fig 4: normalized circumferential stress distribution ($\omega = 500\,\mathrm{rad}/s$)

In Fig 5, the radial displacements across three layers along the thickness direction are shown at points distant from the boundaries. These displacements decrease along the length, with values reducing from the inner layer to the outer layer.

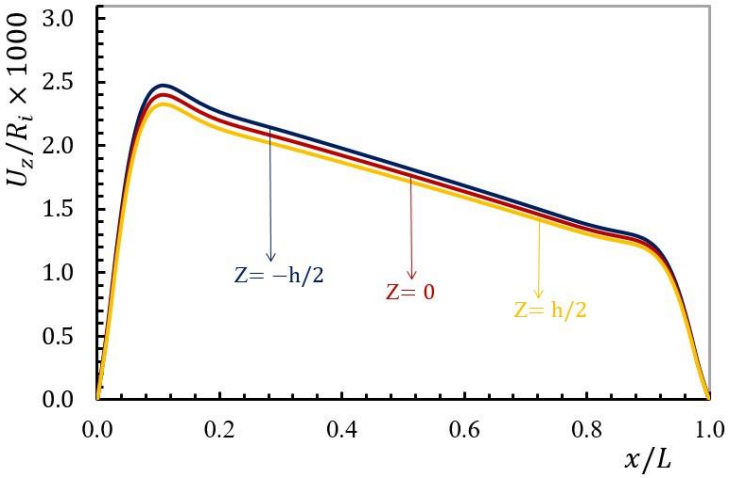

Fig 5: normalized radial displacement distribution in different layers ($\omega = 500\,\mathrm{rad}/s$)

In Fig 6, the graph illustrates circumferential stress values across three layers in the thickness direction, at locations far from the boundaries. The stress values diminish from the inner layer to the outer layer. The variations in stress values along the longitudinal direction are decreasing. The slope of these variations decreases from the inner layer towards the outer layer.

In Fig 7, the distribution of shear stress along the length of the cylindrical shells is illustrated. As depicted, shear stress values can be neglected across all layers and at points away from the boundaries.

In Fig 8, the distribution of dimensionless equivalent stress (von-Mises) across three layers along the thickness direction, away from the boundaries, is illustrated. The values exhibit a decreasing trend along the longitudinal direction. Moreover, the slope of this decrease diminishes from the inner layer to the outer layer. The stress values decrease from the inner layer to the outer layer.

Figs 9-11 illustrate the changes in displacement values and stresses within the intermediate layer at different angular velocities. Fig 9 specifically focuses on the changes in dimensionless radial displacement along the longitudinal direction for various angular velocities. The radial displacement profiles exhibit a decreasing trend along the longitudinal direction. while the profile shape remains largely consistent across different angular velocities, the magnitude of displacement increases with increasing angular velocity.

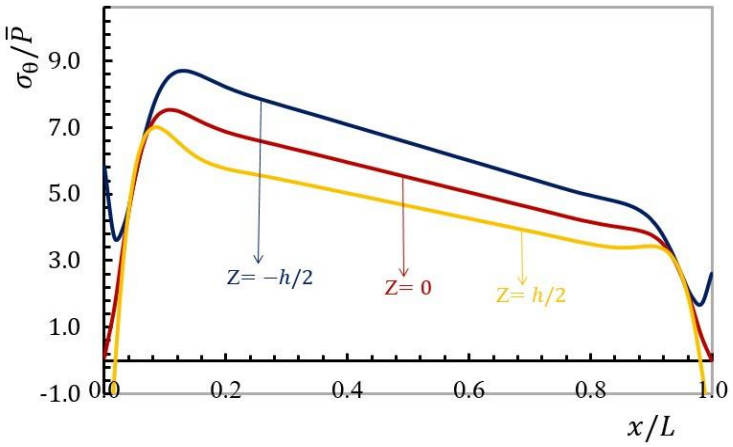

Fig 6: normalized circumferential stress distribution in different layers ($\omega = 500\,\mathrm{rad}/s$)

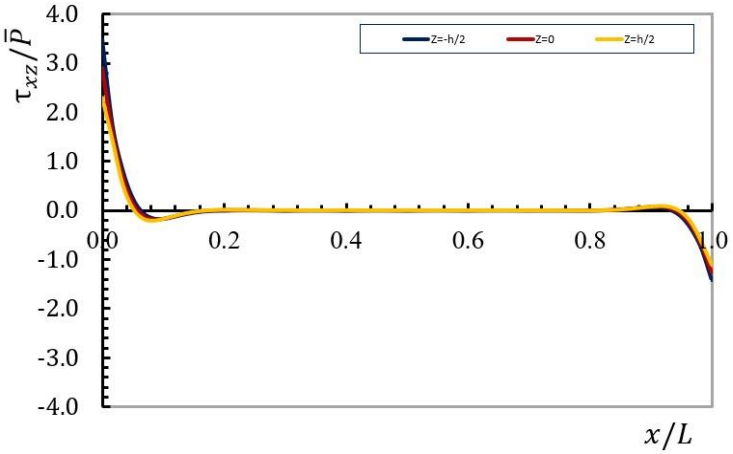

Fig 7: Normalized shear stress distribution in different layers ($\omega = 500\,\mathrm{rad}/s$)

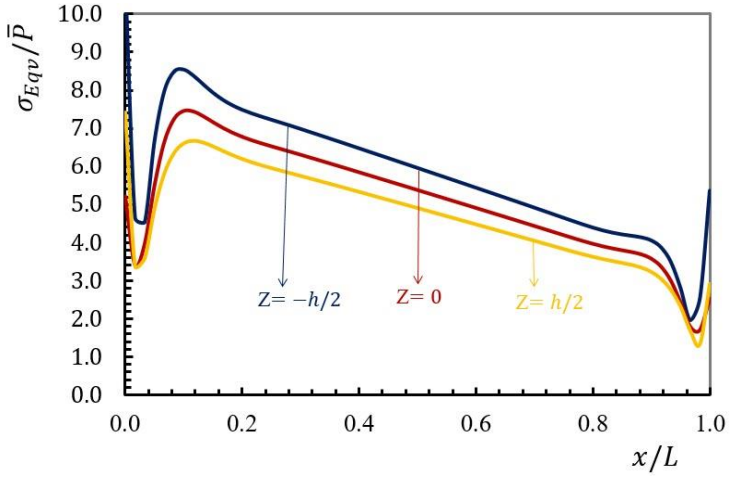

Fig 8: normalized equivalent stress distribution in different layers ($\omega = 500\,\mathrm{rad}/s$)

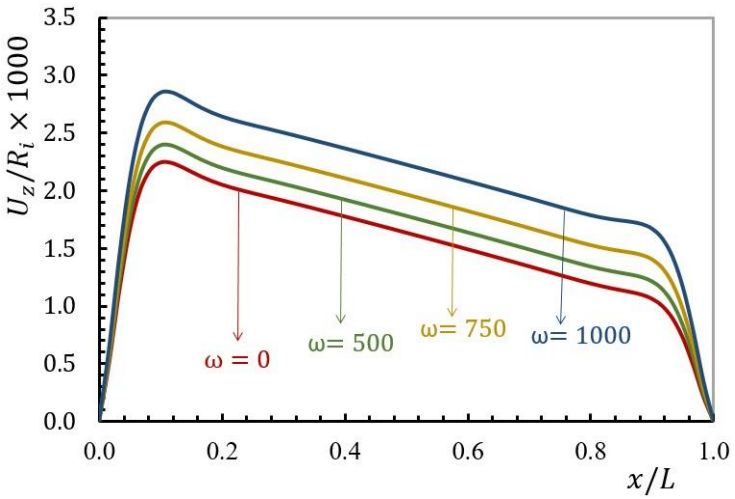

Fig 9: normalized radial displacement distribution subjected to different angular velocity ($h = 0$)

Fig 10 illustrates the variation of circumferential stress within the intermediate layer at different angular velocities. These stress values exhibit nearly similar profiles, increasing with increasing angular velocities and exhibiting a steep decreasing trend along the longitudinal direction.

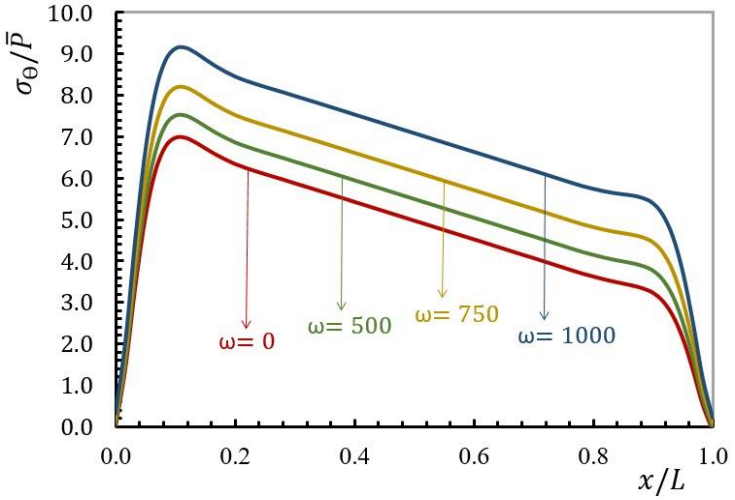

Fig 10: normalized circumferential stress distribution subjected to different angular velocity ($h = 0$)

Fig 11 presents shear stress values within the intermediate layer at various angular velocities. However, for further analysis, these values may be negligible and can be disregarded.

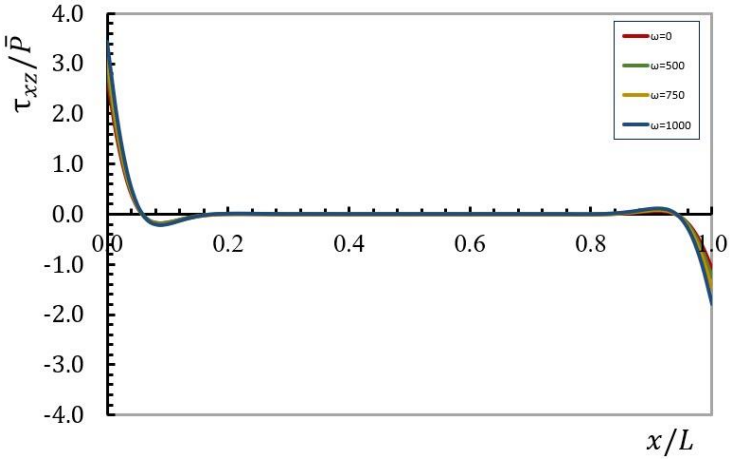

Fig 11: normalized shear stress distribution subjected to different angular velocity ($h = 0$)

Fig 12 presents the variation of equivalent stress values within the intermediate layer at different angular velocities. These stress values exhibit nearly similar profiles, increasing with increasing angular velocities. Notably, the presented graph reveals a noticeable decreasing trend along the longitudinal direction.

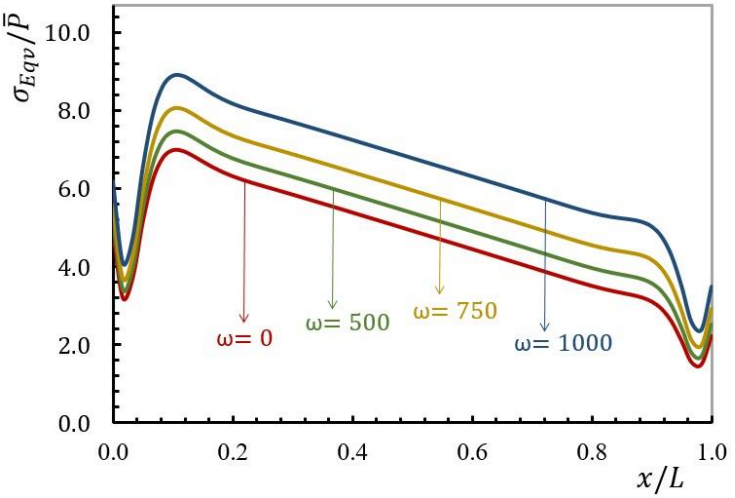

Fig 12: normalized equivalent stress distribution subjected to different angular velocity ($h = 0$)

6. Conclusion

This study provides a detailed examination of the stress and displacement distributions within cylindrical shells. The findings indicate that both circumferential and radial stresses and displacements exhibit decreasing trends from the inner layer to the outer layer and along the longitudinal direction. The FEM results show a good correlation with this method, validating the analysis. Additionally, shear stress values are negligible across all layers away from the boundaries, simplifying the overall stress profile. Furthermore, the impact of angular velocity on the intermediate layer is significant, with increased radial displacement and circumferential stress values at higher angular velocities. However, these stresses still follow a decreasing trend longitudinally. A comprehensive understanding of these stress and displacement behaviours is crucial for optimizing the design and ensuring the structural integrity of cylindrical shells under various operating conditions.

References

[1] P. Fatehi, M. Z. Nejad, Effects of material gradients on onset of yield in FGM rotating thick cylindrical shells, *International Journal of Applied Mechanics*, Vol. 6, No. 04, pp. 1450038, 2014.

[2] Z. Mazarei, M. Z. Nejad, A. Hadi, Thermo-elasto-plastic analysis of thick-walled spherical pressure vessels made of functionally graded materials, *International Journal of Applied Mechanics*, Vol. 8, No. 04, pp. 1650054, 2016.

[3] M. Zamani Nejad, M. Jabbari, A. Hadi, A review of functionally graded thick cylindrical and conical shells, *Journal of Computational Applied Mechanics*, Vol. 48, No. 2, pp. 357-370, 2017.

[4] A. Farajpour, A. Rastgoo, Size-dependent static stability of magneto-electro-elastic CNT/MT-based composite nanoshells under external electric and magnetic fields, *Microsystem Technologies*, Vol. 23, pp. 5815-5832, 2017.

[5] T. Ebrahimi, M. Z. Nejad, H. Jahankohan, A. Hadi, Thermoelastoplastic response of FGM linearly hardening rotating thick cylindrical pressure vessels, *Steel and Composite Structures, An International Journal*, Vol. 38, No. 2, pp. 189-211, 2021.

[6] M. Z. Nejad, A. Rastgoo, A. Hadi, Exact elasto-plastic analysis of rotating disks made of functionally graded materials, *International Journal of Engineering Science*, Vol. 85, pp. 47-57, 2014.

[7] A. Afshin, M. Zamani Nejad, K. Dastani, Transient thermoelastic analysis of FGM rotating thick cylindrical pressure vessels under arbitrary boundary and initial conditions, *Journal of Computational Applied Mechanics*, Vol. 48, No. 1, pp. 15-26, 2017.

[8] M. Kashkoli, K. N. Tahan, M. Nejad, Time-dependent creep analysis for life assessment of cylindrical vessels using first order shear deformation theory, *Journal of Mechanics*, Vol. 33, No. 4, pp. 461-474, 2017.

[9] M. Gharibi, M. Zamani Nejad, A. Hadi, Elastic analysis of functionally graded rotating thick cylindrical pressure vessels with exponentially-varying properties using power series method of Frobenius, *Journal of Computational Applied Mechanics*, Vol. 48, No. 1, pp. 89-98, 2017.

[10] M. Z. Nejad, T. Taghizadeh, S. J. Mehrabadi, S. Herasati, Elastic analysis of carbon nanotube-reinforced composite plates with piezoelectric layers using shear deformation theory, *International Journal of Applied Mechanics*, Vol. 9, No. 01, pp. 1750011, 2017.

[11] M. D. Kashkoli, K. N. Tahan, M. Z. Nejad, Time-dependent thermomechanical creep behavior of FGM thick hollow cylindrical shells under non-uniform internal pressure, *International Journal of Applied Mechanics*, Vol. 9, No. 06, pp. 1750086, 2017.

[12] M. Jabbari, M. Z. Nejad, Mechanical and thermal stresses in radially functionally graded hollow cylinders with variable thickness due to symmetric loads, *Australian Journal of Mechanical Engineering*, 2018.

[13] M. H. Dindarloo, L. Li, Vibration analysis of carbon nanotubes reinforced isotropic doubly-curved nanoshells using nonlocal elasticity theory based on a new higher order shear deformation theory, *Composites Part B: Engineering*, Vol. 175, pp. 107170, 2019.

[14] T. Taghizadeh, M. Z. Nejad, M. D. Kashkoli, Thermo-Elastic Creep Analysis and Life Assessment of Thick Truncated Conical Shells with Variable Thickness, *International Journal of Applied Mechanics*, Vol. 11, No. 09, pp. 1950086, 2019.

[15] A. H. Sofiyev, F. Dikmen, Buckling Analysis of Functionally Graded Shells under Mixed Boundary Conditions Subjected to Uniform Lateral Pressure, *Journal of Applied and Computational Mechanics*, Vol. 7, No. 1, pp. 345-354, 2021.

[16] T. Taghizadeh, M. Zamani Nejad, Thermo-elastic creep analysis and life assessment of rotating thick pressurized cylindrical shells using third-order shear deformation theory, *Journal of Computational Applied Mechanics*, Vol. 52, No. 3, pp. 366-393, 2021.

[17] M. Jabbari, M. Zamani Nejad, Electro-mechanical Analysis of Rotating Cylinder Made of Functionally Graded Piezoelectric Materials: Sensor and Actuator, *Amirkabir Journal of Mechanical Engineering*, Vol. 51, No. 1, pp. 215-224, 2019.

[18] M. D. Kashkoli, K. N. Tahan, M. Z. Nejad, Creep damage and life assessment of thick cylindrical pressure vessels with variable thickness made of 304L austenitic stainless steel, *Steel and Composite Structures*, Vol. 32, No. 6, pp. 701, 2019.

[19] M. Nejad, Z. Hoseini, A. Niknejad, M. Ghannad, Steady-state creep deformations and stresses in FGM rotating thick cylindrical pressure vessels, *Journal of Mechanics*, Vol. 31, No. 1, pp. 1-6, 2015.

[20] M. D. Kashkoli, M. Z. Nejad, Time-dependent thermo-elastic creep analysis of thick-walled spherical pressure vessels made of functionally graded materials, *Journal of Theoretical and applied Mechanics*, Vol. 53, No. 4, pp. 1053-1065, 2015.

[21] M. Z. Nejad, P. Fatehi, Exact elasto-plastic analysis of rotating thick-walled cylindrical pressure vessels made of functionally graded materials, *International Journal of Engineering Science*, Vol. 86, pp. 26-43, 2015.

[22] M. Z. Nejad, M. D. Kashkoli, Time-dependent thermo-creep analysis of rotating FGM thick-walled cylindrical pressure vessels under heat flux, *International Journal of Engineering Science*, Vol. 82, pp. 222-237, 2014.

[23] M. Dehghan, M. Z. Nejad, A. Moosaie, Thermo-electro-elastic analysis of functionally graded piezoelectric shells of revolution: Governing equations and solutions for some simple cases, *International Journal of Engineering Science*, Vol. 104, pp. 34-61, 2016.

[24] M. D. Kashkoli, M. Z. Nejad, Time-dependent creep analysis and life assessment of 304 L austenitic stainless steel thick pressurized truncated conical shells, *Steel and Composite Structures, An International Journal*, Vol. 28, No. 3, pp. 349-362, 2018.

[25] M. Z. Nejad, N. Alamzadeh, A. Hadi, Thermoelastoplastic analysis of FGM rotating thick cylindrical pressure vessels in linear elastic-fully plastic condition, *Composites Part B: Engineering*, Vol. 154, pp. 410-422, 2018.

[26] A. Farajpour, A. Rastgoo, M. Farajpour, Nonlinear buckling analysis of magneto-electro-elastic CNT-MT hybrid nanoshells based on the nonlocal continuum mechanics, *Composite Structures*, Vol. 180, pp. 179-191, 2017.

[27] L. Li, X. Li, Y. Hu, Nonlinear bending of a two-dimensionally functionally graded beam, *Composite Structures*, Vol. 184, pp. 1049-1061, 2018/01/15/, 2018.

[28] M. Z. Nejad, G. Rahimi, M. Ghannad, Set of field equations for thick shell of revolution made of functionally graded materials in curvilinear coordinate system, *Mechanics*, Vol. 77, No. 3, pp. 18-26, 2009.
[29] M. Ghannad, M. Z. Nejad, Elastic analysis of pressurized thick hollow cylindrical shells with clamped-clamped ends, *Mechanics*, Vol. 85, No. 5, pp. 11-18, 2010.
[30] Y.-W. Zhang, G.-L. She, Nonlinear primary resonance of axially moving functionally graded cylindrical shells in thermal environment, *Mechanics of Advanced Materials and Structures*, pp. 1-13, 2023.
[31] F. Ramezani, M. Z. Nejad, Thermoelastic analysis of rotating FGM thick-walled cylindrical pressure vessels under bi-directional thermal loading using disk-form multilayer, *Steel and Composite Structures*, Vol. 51, No. 2, pp. 139, 2024.
[32] I. Panferov, Stresses in a transversely isotropic conical elastic pipe of constant thickness under a thermal load, *Journal of Applied Mathematics and Mechanics*, Vol. 56, No. 3, pp. 410-415, 1992.
[33] B. Sundarasivarao, N. Ganesan, Deformation of varying thickness of conical shells subjected to axisymmetric loading with various end conditions, *Engineering fracture mechanics*, Vol. 39, No. 6, pp. 1003-1010, 1991.
[34] I. Mirsky, G. Herrmann, Axially symmetric motions of thick cylindrical shells, 1958.
[35] F. Witt, Thermal stress analysis of conical shells, *Nuclear Structural Engineering*, Vol. 1, No. 5, pp. 449-456, 1965.
[36] K. Jane, Y. Wu, A generalized thermoelasticity problem of multilayered conical shells, *International Journal of Solids and Structures*, Vol. 41, No. 9-10, pp. 2205-2233, 2004.
[37] H. R. Eipakchi, S. Khadem, G. Rahimi S, Axisymmetric stress analysis of a thick conical shell with varying thickness under nonuniform internal pressure, *Journal of engineering mechanics*, Vol. 134, No. 8, pp. 601-610, 2008.
[38] M. Z. Nejad, G. Rahimi, Deformations and stresses in rotating FGM pressurized thick hollow cylinder under thermal load, *Scientific Research and Essays*, Vol. 4, No. 3, pp. 131-140, 2009.
[39] M. Ghannad, M. Z. Nejad, G. Rahimi, Elastic solution of axisymmetric thick truncated conical shells based on first-order shear deformation theory, *Mechanics*, Vol. 79, No. 5, pp. 13-20, 2009.
[40] M. Jabbari, M. Zamani Nejad, M. Ghannad, Stress analysis of rotating thick truncated conical shells with variable thickness under mechanical and thermal loads, *Journal of Solid Mechanics*, Vol. 9, No. 1, pp. 100-114, 2017.
[41] M. Ghannad, M. Z. Nejad, Elastic solution of pressurized clamped-clamped thick cylindrical shells made of functionally graded materials, *Journal of theoretical and applied mechanics*, Vol. 51, No. 4, pp. 1067-1079, 2013.
[42] H. R. Eipakchi, Third-order shear deformation theory for stress analysis of a thick conical shell under pressure, *Journal of Mechanics of materials and structures*, Vol. 5, No. 1, pp. 1-17, 2010.
[43] M. Ghannad, G. H. Rahimi, M. Z. Nejad, Determination of displacements and stresses in pressurized thick cylindrical shells with variable thickness using perturbation technique, *Mechanics*, Vol. 18, No. 1, pp. 14-21, 2012.
[44] M. Z. Nejad, M. Jabbari, M. Ghannad, Elastic analysis of rotating thick cylindrical pressure vessels under non-uniform pressure: linear and non-linear thickness, *Periodica Polytechnica Mechanical Engineering*, Vol. 59, No. 2, pp. 65-73, 2015.
[45] Ö. Civalek, Vibration analysis of laminated composite conical shells by the method of discrete singular convolution based on the shear deformation theory, *Composites Part B: Engineering*, Vol. 45, No. 1, pp. 1001-1009, 2013.
[46] M. Zamani Nejad, M. Jabbari, M. Ghannad, Elastic analysis of rotating thick truncated conical shells subjected to uniform pressure using disk form multilayers, *International Scholarly Research Notices*, Vol. 2014, 2014.
[47] M. Z. Nejad, M. Jabbari, M. Ghannad, A semi-analytical solution of thick truncated cones using matched asymptotic method and disk form multilayers, *Archive of Mechanical Engineering*, Vol. 61, No. 3, pp. 495--513, 2014.
[48] M. Ghannad, M. Jabbari, M. Nejad, An elastic analysis for thick cylindrical pressure vessels with variable thickness, *Engineering Solid Mechanics*, Vol. 3, No. 2, pp. 117-130, 2015.
[49] M. Jabbari, M. Z. Nejad, M. Ghannad, Thermo-elastic analysis of axially functionally graded rotating thick cylindrical pressure vessels with variable thickness under mechanical loading, *International journal of engineering science*, Vol. 96, pp. 1-18, 2015.
[50] M. Z. Nejad, M. Jabbari, M. Ghannad, Elastic analysis of axially functionally graded rotating thick cylinder with variable thickness under non-uniform arbitrarily pressure loading, *International Journal of Engineering Science*, Vol. 89, pp. 86-99, 2015.

[51] M. Jabbari, N. M. ZAMANI, M. Ghannad, Thermoelastic analysis of rotating thick truncated conical shells subjected to non-uniform pressure, 2016.

[52] M. D. Kashkoli, K. N. Tahan, M. Z. Nejad, Thermomechanical creep analysis of FGM thick cylindrical pressure vessels with variable thickness, *International Journal of Applied Mechanics,* Vol. 10, No. 01, pp. 1850008, 2018.

[53] A. A. Hamzah, H. K. Jobair, O. I. Abdullah, E. T. Hashim, L. A. Sabri, An investigation of dynamic behavior of the cylindrical shells under thermal effect, *Case studies in thermal engineering,* Vol. 12, pp. 537-545, 2018.

[54] M. Ghannad, G. H. Rahimi, M. Z. Nejad, Elastic analysis of pressurized thick cylindrical shells with variable thickness made of functionally graded materials, *Composites Part B: Engineering,* Vol. 45, No. 1, pp. 388-396, 2013.

[55] F. Aghaienezhad, R. Ansari, M. Darvizeh, On the Stability of Hyperelastic Spherical and Cylindrical Shells Subjected to External Pressure Using a Numerical Approach, *International Journal of Applied Mechanics,* Vol. 14, No. 10, pp. 2250094, 2022.

[56] M. Z. Nejad, M. Jabbari, M. Ghannad, A general disk form formulation for thermo-elastic analysis of functionally graded thick shells of revolution with arbitrary curvature and variable thickness, *Acta Mechanica,* Vol. 228, pp. 215-231, 2017.

[57] O. Ifayefunmi, D. Ruan, Buckling of Stiffened Cone–Cylinder Structures Under Axial Compression, *International Journal of Applied Mechanics,* Vol. 14, No. 07, pp. 2250075, 2022.

[58] H. Gharooni, M. Ghannad, M. Z. Nejad, Thermo-elastic analysis of clamped-clamped thick FGM cylinders by using third-order shear deformation theory, *Latin American Journal of Solids and Structures,* Vol. 13, pp. 750-774, 2016.

[59] F. Ramezani, M. Z. Nejad, M. Ghannad, Thermoelastic analysis of rotating thick-walled cylindrical pressure vessels with linear variable thickness under bi-directional temperature, *Journal of Computational Applied Mechanics,* Vol. 54, No. 4, pp. 515-532, 2023.

[60] M. Z. Nejad, M. Jabbari, M. Ghannad, Elastic analysis of FGM rotating thick truncated conical shells with axially-varying properties under non-uniform pressure loading, *Composite Structures,* Vol. 122, pp. 561-569, 2015.

[61] F. Ramezani, M. Z. Nejad, M. Ghannad, Bi-Directional Thermo-Elastic Analysis of Pressurized Thick Cylindrical Shell with Nonlinear Variable Thickness, *Journal of Computational Applied Mechanics,* Vol. 55, No. 1, pp. 125-143, 2024.

[62] S. Mannani, L. Collini, M. Arefi, Mechanical stress and deformation analyses of pressurized cylindrical shells based on a higher-order modeling, *Defence Technology,* Vol. 20, pp. 24-33, 2023.

[63] S. Vlachoutsis, Shear correction factors for plates and shells, *International Journal for Numerical Methods in Engineering,* Vol. 33, No. 7, pp. 1537-1552, 1992.